Exciton radiative lifetime in transition metal dichalcogenide monolayers

Cédric Robert, David Lagarde, Fabian Cadiz, Gang Wang, Benjamin Lassagne, Thierry Amand, Andrea Balocchi, Pierre Renucci, S. Tongay, B. Urbaszek, et al.

Exciton radiative lifetime in transition metal dichalcogenide monolayers

C. Robert,[1] D. Lagarde,[1] F. Cadiz,[1] G. Wang,[1] B. Lassagne,[1] T. Amand,[1] A. Balocchi,[1] P. Renucci,[1] S. Tongay,[2] B. Urbaszek,[1] and X. Marie[1]

[1]*Université de Toulouse, INSA-CNRS-UPS, LPCNO, 135 Ave. de Rangueil, 31077 Toulouse, France*

[2]*School for Engineering of Matter, Transport and Energy, Arizona State University, Tempe, Arizona 85287, USA*

(Received 1 March 2016; published 12 May 2016)

We have investigated the exciton dynamics in transition metal dichalcogenide monolayers using time-resolved photoluminescence experiments performed with optimized time resolution. For $MoSe_2$ monolayer, we measure $\tau^0_{rad} = 1.8 \pm 0.2$ ps at $T = 7$ K that we interpret as the intrinsic radiative recombination time. Similar values are found for WSe_2 monolayers. Our detailed analysis suggests the following scenario: at low temperature ($T \lesssim 50$ K), the exciton oscillator strength is so large that the entire light can be emitted before the time required for the establishment of a thermalized exciton distribution. For higher lattice temperatures, the photoluminescence dynamics is characterized by two regimes with very different characteristic times. First the photoluminescence intensity drops drastically with a decay time in the range of the picosecond driven by the escape of excitons from the radiative window due to exciton-phonon interactions. Following this first nonthermal regime, a thermalized exciton population is established gradually yielding longer photoluminescence decay times in the nanosecond range. Both the exciton effective radiative recombination and nonradiative recombination channels including exciton-exciton annihilation control the latter. Finally the temperature dependence of the measured exciton and trion dynamics indicates that the two populations are not in thermodynamical equilibrium.

DOI: 10.1103/PhysRevB.93.205423

I. INTRODUCTION

Transition metal dichalcogenides (TMDCs) such as MX_2 (M = Mo, W; X = S, Se, Te) are a new exciting class of atomically flat, two-dimensional materials for electronics and optoelectronics. In contrast to graphene, monolayer MX_2 have a direct band gap yielding interesting luminescence properties in the visible region of the optical spectrum [1,2]. This has been exploited to fabricate light-emitting diodes and laser prototypes using TMDC monolayer as active region [3–7]. The combined presence of inversion symmetry breaking and strong spin-orbit coupling in these monolayers (MLs) also yields very original spin/valley properties, which are usually probed by optical spectroscopy techniques [8–12].

Recent experimental and theoretical studies also demonstrated that the optical properties of ML TMDC are governed by strongly bound excitons with binding energy of the order of 500 meV [13–19]. This is very promising for possible applications based on strong light-matter coupling [20,21]. Therefore the knowledge of the exciton lifetime in these new two-dimensional (2D) semiconductors is crucial from both a fundamental and applied physics point of view.

The exciton and carrier dynamics in TMDC monolayers has been investigated by pump-probe absorption or reflectivity experiments [22–27]. Thanks to very good time resolution (∼100 fs), these experiments evidenced complex dynamics usually described by multiexponential decay times [28]. However the identification of radiative recombination times among the multiple mechanisms of collective electronic excitations in the transient absorption or reflectivity spectra is usually challenging [26]. The ideal spectroscopy tool to investigate the radiative recombination properties is time-resolved photoluminescence (TRPL). Nevertheless it is usually characterized by a modest time resolution (∼ tens of ps) that can prevent the observation of key features associated with fast radiative recombination times [29–31]. At low temperature ($T \lesssim 10$ K), recent TRPL measurements in MoS_2, $MoSe_2$, and WSe_2 MLs evidenced a very fast emission decay time of ∼3–5 ps limited by the time resolution of the setup [32–35]. Though exciton radiative recombination times in the range 0.1–1 ps have been calculated [36,37], a nonambiguous measurement of the exciton radiative recombination in TMDC monolayers is still lacking.

Here we present a comprehensive investigation of the exciton dynamics using high-resolution time-resolved photoluminescence technique. These experiments reveal the transient evolution from a nonthermal regime where the population decay is dominated by the intrinsic exciton radiative recombination to a thermalized exciton distribution where both radiative and nonradiative recombination channels have to be considered. As a model system, we present a detailed investigation of the $MoSe_2$ ML from T = 7–300 K, where the neutral and charged exciton PL signals are not obscured by defects-related emission. Measurements on WSe_2 ML are also discussed. In order to draw some general conclusions we have investigated $MoSe_2$ ML exfoliated from different bulk materials and with different environment (suspended or directly deposited on SiO_2/Si substrate). This allows us to distinguish between intrinsic or extrinsic recombination mechanisms.

Thanks to an optimized time resolution of the setup based on a sub-ps streak camera and the quasiresonant excitation of the exciton ground state we managed to resolve the intrinsic exciton radiative recombination time which dominates the exciton decay in the temperature range T = 7–50 K. We find $\tau^0_{rad} = 1.8 \pm 0.2$ ps in $MoSe_2$ ML for $T = 7$ K. For larger temperatures, the initial decay time decreases to sub-ps values as a consequence of the escape time of exciton out of the radiative window due to exciton-phonon interactions. Longer recombination times (∼ns) are measured after this initial transient when thermalized excitons can be considered. This

longer decay time is controlled by the effective exciton radiative recombination time, the interplay between bright and dark fine-structure excitons [30,38–40] and the nonradiative recombination channels including the exciton-exciton annihilation rate [29,41]. Finally the simultaneous measurement of the exciton and trion dynamics as a function of temperature or resident carrier concentrations lead us to the conclusion that the two populations are not in thermodynamical equilibrium in contrast to recent assumptions [30,42].

The paper is organized as follows. The next section presents the samples characteristics and the experimental setup. Then we discuss the theoretical background of the radiative recombination of Wannier-Mott excitons in 2D semiconductors (Sec. III). The measurements of the very fast PL decay time associated with the exciton intrinsic radiative recombination times are presented in Sec. IV. The dependence of the thermalized excitons kinetics as a function of temperature is discussed in Sec. V with all the radiative and nonradiative mechanisms. Finally the trion radiative recombination time is measured in Sec. VI. The drastic decrease of trion photoluminescence decay time with temperature and its dependence on the resident carrier density are discussed. Finally we discuss in Sec. VII several issues related to the exciton formation process: the free versus localized exciton dynamics and the key role played by the different nonoptically active (dark) exciton states.

II. SAMPLES AND EXPERIMENTAL SETUPS

$MoSe_2$ and WSe_2 ML flakes are obtained by micromechanical cleavage of bulk crystals on SiO_2/Si substrates using viscoelastic stamping [35,43]. The ML region is identified by optical contrast and very clearly in PL spectroscopy. We present in this paper the results obtained on four different ML flakes: ML A and ML B are obtained with $MoSe_2$ bulk materials from 2D semiconductors company and Arizona State University respectively. The latter was grown using low-pressure vapor transport (LPVT) technique to achieve high optical quality materials [35,38]. $MoSe_2$ ML C is suspended between two Cr/Au (5/50 nm) electrodes prepatterned by *e*-beam lithography on SiO_2(90 nm)/Si substrate [see the sketch of Fig. 7(a)]. The distance between the two electrodes is 4 μm (i.e., larger than the laser spot). The application of a bias voltage between the top Cr/Au electrodes and the *p*-doped Si substrate (used as back gate) enables us to tune electrically the resident carrier density. For comparison, we also investigated a WSe_2 ML flake (ML D) obtained from bulk material from 2D semiconductors and transferred onto a simple SiO_2/Si substrate. A standard micro-PL setup is used to record the emission dynamics in the temperature range $T = 7$–300 K. The laser excitation and PL detection spot diameters are ≈ 2 μm, i.e., smaller than the ML flake diameter. It is also larger than the estimated exciton diffusion length in TMDC ML [24]. For time-resolved photoluminescence experiments, the flakes are excited by $\sim$150-fs pulses generated by a tunable mode-locked Ti:Sa laser with a repetition rate of 80 MHz. For $MoSe_2$ MLs similar results have been obtained for laser excitation energy 1.779 or 1.746 eV. For WSe_2 ML, the excitation energy was set to 1.797 eV. The laser average power on the flakes lies in the linear-response regime with a typical value of 100 μW. This corresponds to a typical photogenerated exciton density

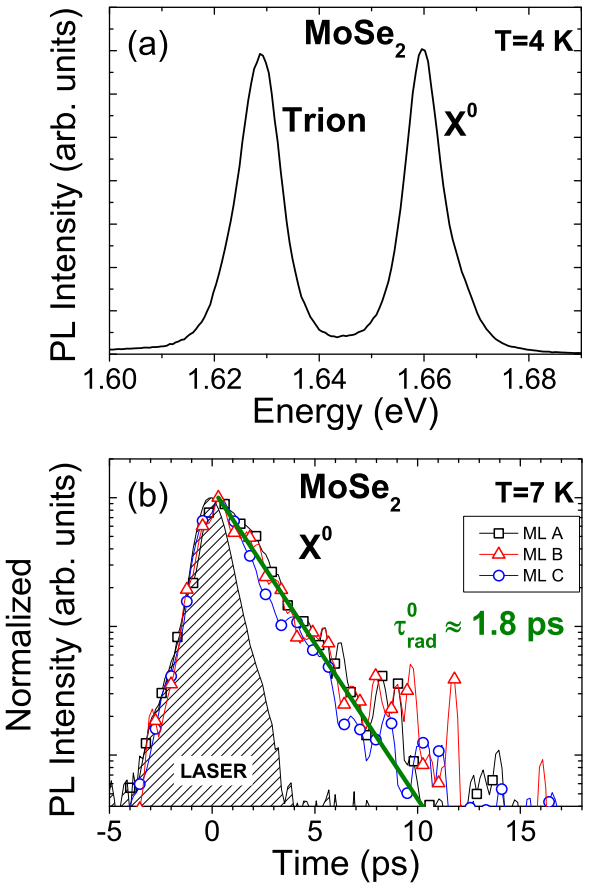

FIG. 1. (a) cw-photoluminescence spectrum of a $MoSe_2$ monolayer (ML A) evidencing the neutral exciton X^0 and the trion (charged exciton) peaks at $T = 4$ K. (b) Time-resolved photoluminescence of three different $MoSe_2$ monolayers following quasiresonant excitation ($E_{exc} = 1.746$ eV) with 150-fs laser pulse; the detection energy corresponds to the X^0 emission (1.66 eV). A monoexponential fit yields $\tau^0_{rad} = 1.8 \pm 0.2$ ps. The instrument response is obtained by detecting the backscattered laser pulse (1.746 eV) on the sample surface, see the hatched area labeled "LASER".

$N_0 \sim 10^{11}$–10^{12} cm^{-2} assuming an absorption of about 1% for the considered excitation wavelengths as roughly estimated from absorption and excitation spectra [43,44]. In all the experiments the excitation laser is linearly polarized. The time resolution of the detection system has been carefully optimized: the PL signal is dispersed by a double spectrometer operating in subtractive mode and detected by a synchro-scan streak camera C10910 with a nominal 900-fs time resolution (full width at half maximum). By measuring the backscattered laser pulse from the sample surface we obtain the overall instrumental response of the time-resolved setup: we find in Fig. 1(b) a characteristic instrument response of 0.8 ps (half width at half maximum) obtained by a Gaussian fit. For cw experiments, the monolayers are excited with a He-Ne laser and the PL emission is dispersed in a spectrometer and detected with a cooled Si–charge-coupled-device (CCD) camera. Figure 1(a) displays the cw PL spectrum of the $MoSe_2$ monolayer (ML A) at $T = 4$ K. Both exciton and trion (charged exciton) peaks are clearly observed as already evidenced in previous works [39,42].

III. EXCITON RADIATIVE LIFETIME: THEORETICAL BACKGROUND

The intrinsic radiative decay of a free Wannier-Mott exciton in 2D semiconductors is due to coupling with a continuum of photon states. For light propagating perpendicular to the 2D layer, this intrinsic radiative decay can be calculated assuming conservation of the in-plane wave vector k. In a simple approach, the exciton intrinsic radiative decay time writes [45,46]

$$\tau^0_{\rm rad} = \frac{1}{2\Gamma_0} = \frac{\hbar\varepsilon}{2k_0}\left(\frac{E_{X^0}}{e\hbar v}\right)^2 \left(a_B^{2D}\right)^2, \quad (1)$$

where Γ_0 is the radiative decay rate, $k_0 = E_{X^0}\sqrt{\varepsilon}/(\hbar c)$ is the light wave-vector in the sample (c is the speed of light, ε is the dielectric constant, and E_{X^0} is the exciton transition energy; v is the Kane velocity related to the interband matrix element of the electron momentum). The 2D exciton Bohr radius is $a_B^{2D} = (\varepsilon\hbar^2)/(4\mu e^2)$ with μ the exciton reduced mass defined as $1/\mu = 1/m_e + 1/m_h$, $m_e(m_h)$ are the effective mass for electron (hole) in the K valleys.

For times longer than typical exciton-exciton and exciton-phonon interaction times, a thermalized exciton population can be considered. Then the decay rate of the exciton photoluminescence is given by the thermal average of the exciton decay rate. It will depend on the thermal energy k_BT and the kinetic energy of the excitons which decay radiatively (in the so called optical window). The latter is at most $E_0 = (\hbar k_0)^2/2M$, where $M = m_e + m_h$ is the exciton mass [see Fig. 4(a)]. Using $M = 1.0\,m_0$ obtained from DFT-G_0W_0 calculations [43] ($m_e = 0.49m_0$ and $m_h = 0.52m_0$, m_0 is the free-electron mass) and n the refractive $n = \sqrt{\varepsilon} \sim 2.2$, we find $E_0 \sim 10\,\mu$eV.

Only the small fraction of exciton which occupies the states with $k < k_0$ (i.e., with kinetic energy smaller than E_0) can decay radiatively. As a consequence, the effective exciton decay time at a given temperature writes [45]

$$\tau^{\rm eff}_{\rm rad} = \frac{3}{2}\frac{k_BT}{E_0}\tau^0_{\rm rad}. \quad (2)$$

We emphasize that this simple expression is valid for $k_BT \gg \gamma_h, E_0$, i.e., a few tens of K in our case (γ_h is the exciton homogeneous linewidth [47]). Equation (2) also considers an averaging over all the fine-structure (bright and dark) exciton spin states. As a consequence it should apply when k_BT is also of the order of the bright-dark exciton splitting [48–50].

At high lattice temperature, the PL decay time is usually not only dominated by pure radiative recombination but also by nonradiative recombination channels. The time evolution of the exciton population with density N can be described by the simple rate equation

$$\frac{dN}{dt} = -\frac{N}{\tau^{\rm eff}_{\rm rad}} - \frac{N}{\tau_{nr}} - \gamma\frac{N^2}{2}, \quad (3)$$

where τ_{nr} is the nonradiative recombination time corresponding to capture time on defects and γ is the nonradiative exciton-exciton annihilation rate [29,41,51,52]. It has been shown recently that the latter process (Auger type) is dominant at room temperature [53,54].

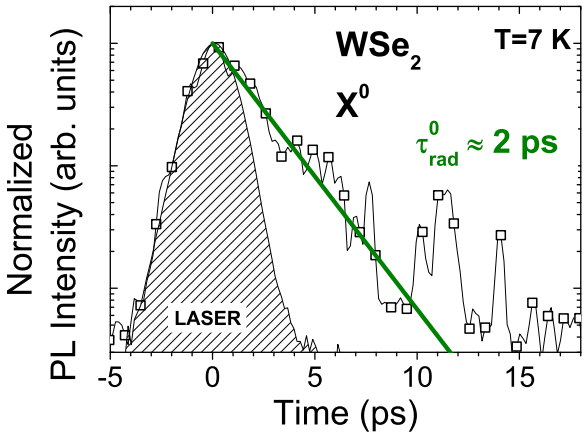

FIG. 2. Time-resolved photoluminescence of a WSe_2 monolayer (ML D) following quasiresonant excitation with 150-fs laser pulse; the excitation and detection energy are 1.797 and 1.751 eV respectively. A monoexponential fit yields 2 ± 0.3 ps.

IV. EXCITON INTRINSIC RADIATIVE LIFETIME

Figure 1(b) displays the photoluminescence dynamics at $T = 7$ K for the three different $MoSe_2$ monolayer samples (MLs A–C). Following a rise time smaller than 1 ps (which cannot be resolved), we observe a monoexponential decay time on more than two orders of magnitude with a characteristic value $\tau^0_{\rm rad} = 1.8 \pm 0.2$ ps. In contrast to previous TRPL measurements limited by a timeresolution of about 3–5 ps [34,35], the PL decay time measured here is clearly longer than the measured instrumental response [see the "laser" curve in Fig. 1(b) for comparison]. A deconvolution procedure using the measured time resolution of the setup does not change significantly the $\tau^0_{\rm rad}$ value. Remarkably Fig. 1(b) shows that the PL decay time is similar for the three samples corresponding to monolayers exfoliated from different $MoSe_2$ bulk materials or with different dielectric environments (suspended or not). This is a strong indication that this decay time corresponds to an intrinsic radiative recombination mechanism and not to nonradiative recombination on defects which are expected to vary from one material to another. Moreover we have measured very similar PL decay times for WSe_2 monolayer (see Fig. 2); a monoexponential fit yields $\tau^0_{\rm rad} \sim 2 \pm 0.2$ ps. Though this low-temperature PL decay time is likely governed by the exciton intrinsic radiative recombination time, we should also consider the possible interplay between the bright and dark excitons (composed of parallel and antiparallel conduction- and valence-band electron spins respectively). It has been shown recently that the dark states lie at lower (higher) energy compared to the bright ones in WSe_2 ($MoSe_2$) monolayers with typical splitting energy of 10–30 meV [30,38–40,50]. For the sake of simplicity, the detailed investigation presented below will be focused on $MoSe_2$ monolayers where we can consider that the transfer from bright (at low energy) to dark states (at high energy) is negligible at low temperatures [50].

Let us emphasize that the laser excitation energy is far below the free-carrier band gap: it lies between the 1-s and 2-s exciton states [43]. The laser excitation energy used here for the $MoSe_2$ monolayers (1.746 eV) corresponds to a difference

between excitation and exciton detection energies of about 90 meV. Considering the large spectral width of the 150-fs laser (∼10 meV), this allows the very fast exciton photogeneration near $k \sim 0$ via a three LO phonon emission process [55,56]. Recent resonant Raman experiments in TMDC monolayers demonstrated clearly the strong efficiency of phonon interaction [57,58].

As a consequence the quasiresonant laser excitation results in the photogeneration of a nonthermal exciton distribution close to $k = 0$ which couples very efficiently to light as all the excitons lie in the radiative window characterized by the energy E_0. This leads to a very efficient and short emission process corresponding to the intrinsic exciton radiative lifetime. The very short intrinsic radiative recombination time (∼10 times shorter than the one measured in GaAs or CdTe quantum wells [59–62]) is the result of the strong oscillator strength associated with the very robust exciton in TMDC ML.

This interpretation is further supported by two arguments:

(i) At $T = 7$ K, all the light is emitted before $t \lesssim 10$ ps. In agreement with previous time-resolved PL measurements in MoS_2, $MoSe_2$, or WSe_2 MLs with lower time resolution [32,34,35], there is no evidence of a second slower decay time following the fast initial one. As observed for higher temperatures (see Sec. V), this would be the fingerprint of a significant fraction of thermalized excitons populating large k wave vectors which do not couple to light [Fig. 4(b)].

(ii) The nonradiative recombination times, clearly evidenced for $T \gtrsim 100$ K (see Sec. V), occur on a much longer time scale (hundreds of ps). As a consequence we propose that the ∼1.8 ps decay time measured in Fig. 1(b) has an intrinsic origin.

The measured exciton decay time can be compared with the calculated intrinsic radiative recombination time of ideal 2D excitons [Eq. (1)]. Using an exciton binding energy of ∼500 meV as measured recently [16,43], the calculated reduced exciton mass $\mu = 0.25m_0$ and the dielectric constant $\varepsilon = 5$ (Ref. [43]), Eq. (1) yields a calculated radiative lifetime of $\tau^0_{\rm rad} \sim 0.3$ ps, six times shorter than the measured one in Fig. 1(b). For this first approximation we have used here the Kane velocity v estimated from a two-band model as $v = \sqrt{E_g/(2m_e)}$, where E_g is the free-carrier band gap [43] (we assume here $m_e = m_h \sim 0.5m_0$). Note that similar sub-ps intrinsic exciton radiative lifetimes values have been obtained with more sophisticated theoretical approaches [36,37]. However these calculated values are based on (i) the assumption of an ideal 2D Wannier-Mott free exciton which is questionable for a 2D material based on TMDC and (ii) several parameters with very large uncertainties including the electron effective mass m_e (which has not been measured yet to the best of our knowledge) and the dielectric constants with complex screening and antiscreening effects [63].

Our measurements can be well interpreted if we assume that the exciton thermalization process requires a characteristic time longer than $\tau^0_{\rm rad}$ for a lattice temperature $T = 7$ K. This thermalization process involves both exciton-exciton and exciton-phonon interactions. For a lattice temperature $T \lesssim 40$ K, the measured initial PL decay time displayed in Fig. 3 does not depend on temperature: in this regime the exciton-phonon interaction time is typically longer than $\tau^0_{\rm rad}$. This absence of variation of the PL decay time in the temperature range 7–40 K (inset of Fig. 3) supports again our interpretation based on a nonthermal exciton distribution. A thermal exciton population should lead to a linear increase of the exciton radiative lifetime with temperature as considered in the low-temperature calculations of Refs. [36,37] [see also Eq. (2)].

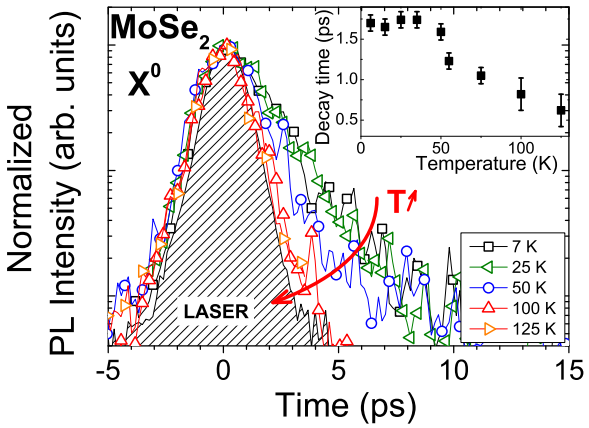

FIG. 3. Temperature dependence of the exciton photoluminescence dynamics for the $MoSe_2$ monolayer (ML A). The excitation energy is $E_{\rm exc} = 1.746$ eV and the detection energy is set to the peak of the X^0 exciton photoluminescence peak. The inset displays the photoluminescence decay time (obtained with a simple monoexponential fit) as a function of temperature.

For larger temperatures ($T \gtrsim 50$ K), we observe that the initial PL decay time decreases. We measured the same temperature dependencies for samples ML B and ML C. We emphasize that we did not observe in this temperature range any blueshift of the PL peak which could have been the fingerprint of a transient change from a localized exciton regime to a free exciton regime [64,65].

In a very simple approach, the PL decay time in this temperature range can be written as $1/\tau_{\rm PL} = 1/\tau^0_{\rm rad} + 1/\tau_{\rm escape}$, where $\tau_{\rm escape}$ is the escape time of excitons from the radiative window driven by the exciton-phonon interaction [Fig. 4(a)]. When the exciton-phonon interaction time becomes shorter than the intrinsic radiative exciton lifetime $\tau^0_{\rm rad}$, the initial PL decay time is no more driven by $\tau^0_{\rm rad}$. For temperatures larger than 125 K, Fig. 3 shows this interaction time becomes so short (<1 ps) that it cannot be resolved any more. The inset in Fig. 3 shows the dependence of $\tau_{\rm PL}$ as a function of temperature. From the measured dependence above 50 K, it should be possible in principle to extract the efficiency of exciton-phonon interactions as recently obtained from 2D Fourier transform spectroscopy in WSe_2 monolayers [47]. In this low-temperature range, only absorption of phonons has to be considered and the scattering rate of $k \sim 0$ excitons outside the radiative window can be described by a linear variation with T [60]. However the limited time resolution in the present TRPL measurements prevent us to extract very accurate values of this exciton-phonon scattering efficiency. Nonlinear techniques such as four-wave mixing experiments in high quality samples will be highly desirable to extract this fundamental parameter [66].

After a few tens of ps, these fast exciton-phonon interactions will yield the establishment of a thermalized Boltzmann

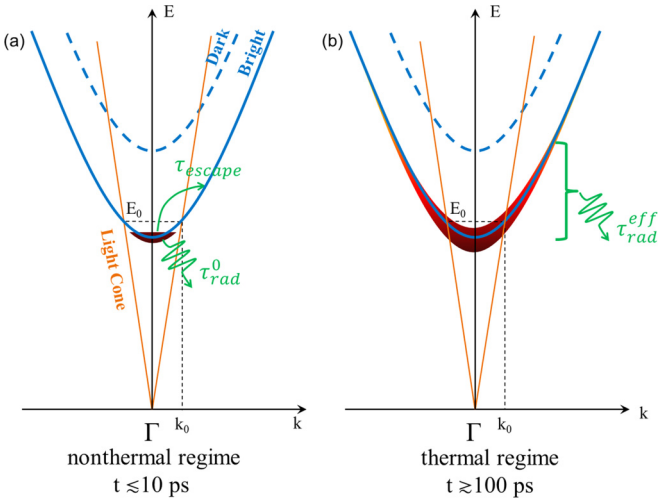

FIG. 4. Schematics of the exciton dispersion curve in the exciton zone center Γ for a $MoSe_2$ monolayer displaying the bright and dark excitons, as well as the radiative light cone characterized by the energy E_0 and the wave vector k_0 (see text). Both the initial nonthermal regime (a) and the thermal one (b) are considered (see text); here the lattice temperature is low enough to consider a negligible population of the Γ-valley dark exciton states.

distribution of exciton and as a consequence longer radiative recombination times [45,60,67].

V. EXCITON EFFECTIVE RADIATIVE LIFETIME

For a thermalized exciton population at a given temperature larger than a few tens of K, the fraction of exciton which lies in the radiative window is small yielding a radiative decay time longer than the intrinsic recombination time [Eq. (2) and Fig. 4(b)]. In the temperature range 100–300 K, we clearly observe in Fig. 5(b) "long" decay times of the order of a ns.

For intermediate temperatures [see, for instance, Fig. 5(a) at $T \sim 125$ K], one can observe in the luminescence dynamics the transition from a nonthermal regime where the fast (∼1 ps) initial decay time probes the fast escape of excitons from the radiative window (discussed in Sec. IV) to a much slower regime with a decay time in the ns range observed at long delay corresponding to the effective radiative lifetime of thermalized excitons [32]. For lattice temperatures above 200 K, Fig. 5(b) shows that the escape time is so fast that the fast decay even disappears. Assuming that the exciton intrinsic radiative lifetime corresponds to the fast PL decay time measured at $T = 7$ K ($\tau^0_{rad} = 1.8$ ps), we get a rough estimate of the exciton effective radiative decay time at $T = 125$ K from Eq. (2): $\tau^{eff}_{rad} \sim 2500$ ps. For $MoSe_2$ ML we used the following parameters: exciton mass $M = 1.0m_0$ and refractive index $n \sim 2.2$ [17,43]. This calculated value is in good agreement with the measured long PL decay time measured in Fig. 5(a).

Although the experimental results are consistent with this exciton effective radiative recombination scenario, a more quantitative analysis cannot be conducted since nonradiative recombination channels have to be considered for temperatures larger than ∼100 K. The inset in Fig. 5(b) displays the variation

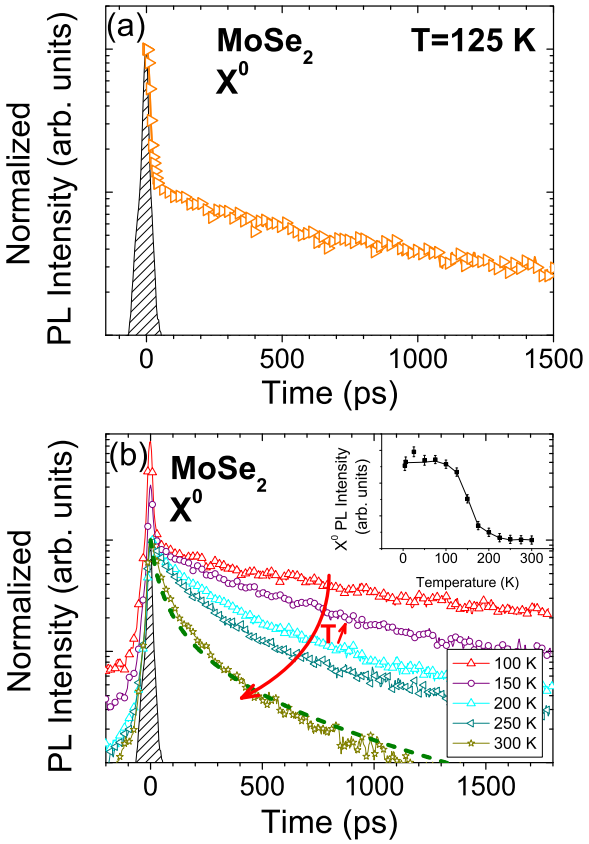

FIG. 5. (a) Exciton photoluminescence dynamics for the $MoSe_2$ monolayer (ML C, $V = 0$ V) at $T = 125$ K. After a fast initial drop by one order of magnitude the luminescence decays with a typical time of the order of ns. The hatched area corresponds to the instrument response time in the same conditions (the time resolution of the Streak Camera for long kinetics is smaller than the one in Figs. 1–3. Consequently the amplitude of the fast initial drop of intensity in this figure is smaller than the one in Fig. 3 for the same temperature). (b) Exciton time-resolved photoluminescence from $T = 100$–300 K. The solid line is a fit of the exciton dynamics at $T = 300$ K using Eq. (3) with the parameters $N_0 = 10^{11}$ cm^{-2}, $1/\tau^{eff}_{rad} + 1/\tau_{nr} = 1$ ns^{-1} and the exciton annihilation rate $\gamma = 0.35$ cm^2/s (see text). The inset presents the temperature dependence of the time-integrated exciton photoluminescence intensity.

of the cw-integrated exciton intensity as a function of temperature. For $7 < T \lesssim 70$ K, the luminescence yield is rather constant: there is no signature of nonradiative recombination channels in agreement with the results presented in Figs. 1–3. In this regime the exciton lifetime is mainly controlled by the very fast exciton intrinsic radiative recombination time τ^0_{rad}. For larger temperatures $T \gtrsim 100$ K, the luminescence yield decreases [inset of Fig. 5(b)] as a significant fraction of excitons lies above the radiative window, their lifetime is much longer and they start to be sensitive to nonradiative recombination channels. Thus the exciton PL decay time measured in Fig. 5(b) for $t \gtrsim 100$ ps (in the thermalized exciton population regime) is controlled both by the exciton effective radiative recombination time τ^{eff}_{rad} and the nonradiative recombination processes [see Eq. (3)].

Figure 5(b) shows that τ_{PL} decreases with the temperature for $T > 100$ K whereas the exciton effective radiative recombination time is expected to increase linearly with T [Eq. (2)]. Note that we measured the same temperature dependencies for ML B obtained with a different bulk $MoSe_2$ material and for ML C which is suspended. We conclude that for $T \gtrsim 100$ K, the main recombination channel for the thermalized exciton population is nonradiative. Two nonradiative recombination processes can be considered: the standard trapping of photogenerated excitons on defects which can be thermally activated and the exciton-exciton annihilation process (Auger type) [29,41]. It has been shown recently [53,68] that the latter is the dominant exciton recombination process at room temperature for photogenerated excitons densities larger than $10^9\,cm^{-2}$. The photoluminescence dynamics presented in Fig. 5 are in agreement with this interpretation. The bold-dashed line in Fig. 5(b) at $T = 300$ K is a fit according to the solution of Eq. (3): $N(t) = N_0 e^{-t/\tau}/[1 + \gamma N_0(1 - e^{-t/\tau})/2]$. Using the exciton-exciton annihilation rate $\gamma = 0.35\,cm^2/s$ recently estimated in $MoSe_2$ ML [29,41], we get a very good agreement with the measured kinetics using the parameters $N_0 = 10^{11}\,cm^{-2}$ and $1/\tau_{rad}^{eff} + 1/\tau_{nr} = 1\,ns^{-1}$. For all temperatures larger than 100 K, the PL decay time is not monoexponential and it has a marked $\sim 1/N$ dependence as expected for the exciton-exciton annihilation process [see Eq. (3)]. We observe that the efficiency of this process increases when the temperature increases as a consequence of the increased mobility of excitons [29,68]. At very low temperature ($T \lesssim 50$ K), the exciton diffusion constant is so small that the exciton-exciton annihilation process efficiency vanishes. Finally we note that Eq. (2) yields a calculated exciton effective radiative lifetime of about 6 ns at room temperature, in good agreement with the recently measured PL decay times in a chemically treated MoS_2 monolayer where nonradiative recombination channels have been suppressed [53,54].

VI. EXCITON AND TRION RADIATIVE LIFETIMES

It is well known that the TMDC monolayers have a significant residual doping density [42]. As a consequence, the PL spectra at low temperature exhibit a clear peak associated with the trion (charged exciton) recombination in addition to the already discussed neutral exciton X^0 peak [see Fig. 1(a)]. In agreement with previous measurements performed in WSe_2 monolayers [34], we did not find in our experiments any evidence of electronic transfer from excitons to trions in $MoSe_2$ ML. For instance, the rise time of the trion luminescence at $T = 7$ K does not correspond to the decay time of the neutral exciton (the improved time resolution used in this work should allow us to easily resolve it). This means that the trion formation time from neutral excitons is longer than the very fast decay of the neutral exciton with the exciton intrinsic radiative recombination time $\tau_{rad}^0 \sim 1.8$ ps [Fig. 1(b)]. A recent investigation based on two-color pump-probe measurements estimated a trion formation time at low temperature of the order of 2 ps in $MoSe_2$ ML [69]. Although this result does not contradict our interpretation, the comparison has to be done with caution because of the different resident carrier densities in the two experiments.

Here the excitons and trions are photogenerated quasiresonantly on a typical scale smaller than 1 ps following 3 and 4 LO phonon emission processes respectively. Note that the exciton-trion energy separation ($\sim$ trion binding energy) coincides with the LO phonon energy [58,70]. Remarkably, our experiments indicate that the exciton and trion populations decay independently.

At $T = 7$ K, we measure in Fig. 6(a) a trion PL decay time of $\sim$15 ps, in agreement with previous reports on WSe_2 or $MoSe_2$ MLs [34,35]. This is also consistent with recent calculations which predict trion radiative recombination times longer than the neutral exciton one [36].

When the temperature increases, Fig. 6(b) shows that the trion integrated PL intensity decreases drastically and it totally vanishes at about 125 K in agreement with previous measurements [42,56]. In these previous works, the relative intensity of exciton and trion line and its dependence as a function of temperature have been analyzed in the framework of a mass action law between excitons, trions, and resident electrons [30,42] with electrons escaping their bound trion state due to thermal fluctuations. However, the corresponding temperature dependence of the PL dynamics has not been measured yet to the best of our knowledge. Figures 6(a) and 6(b) show that the trion PL decay time decreases strongly when T increases. Remarkably it varies from 15 ps at $T = 7$ K down to times smaller than 1 ps at $T > 100$ K. Considering the very different exciton and trion lifetimes measured in this study, the validity of a mass action law to explain the temperature dependence is questionable. Such interpretation based on a thermodynamical equilibrium between excitons, trions, and resident electrons fails to explain the very short trion PL decay time measured at 100 K (at this temperature the exciton decay time measured in exactly the same conditions is of the order of 1 ns, i.e., three orders of magnitude longer than the trion one). An alternative possible explanation could be the following: for temperatures larger than 50 K, the trion PL decay time could be governed by efficient exciton-LO phonon inelastic scattering as recently observed in WSe_2 with a double-Raman resonance between exciton and trion states [58]. When the temperature increases, this process is more and more efficient yielding a shorter decay of the trion luminescence intensity, which is no more driven by the trion radiative recombination time but by the trion-phonon interaction time. The fast decrease of the trion PL decay time induced by this scattering mechanism at large temperature is perfectly consistent with the drop of the trion integrated PL intensity when the temperature increases [see Fig. 6(b)]. Moreover, the activation energy E_A of the decay process extracted from Fig. 6(b) is $E_A = 33 \pm 2$ meV, quite close to both the trion measured binding energy $E_B(X^-) \sim 31 \pm 1$ meV [Figs. 1(a) and 6(b) inset] and optical-phonon energies of IMC (in-plane relative motion of transition metal and chalcogen atoms) and OC (out-of-plane chalcogen vibration) modes ($E_{IMC}^{E'} = 35.8$ meV or $E_{OC}^{A_1'} = 30.0$ meV respectively [71,72]). Once the trion has been dissociated into an exciton and a free electron for temperatures higher than 50 K, the reverse process is very unlikely because the bimolecular trion formation time at high temperature becomes much longer than the exciton lifetime, similarly to what has been clearly evidenced in

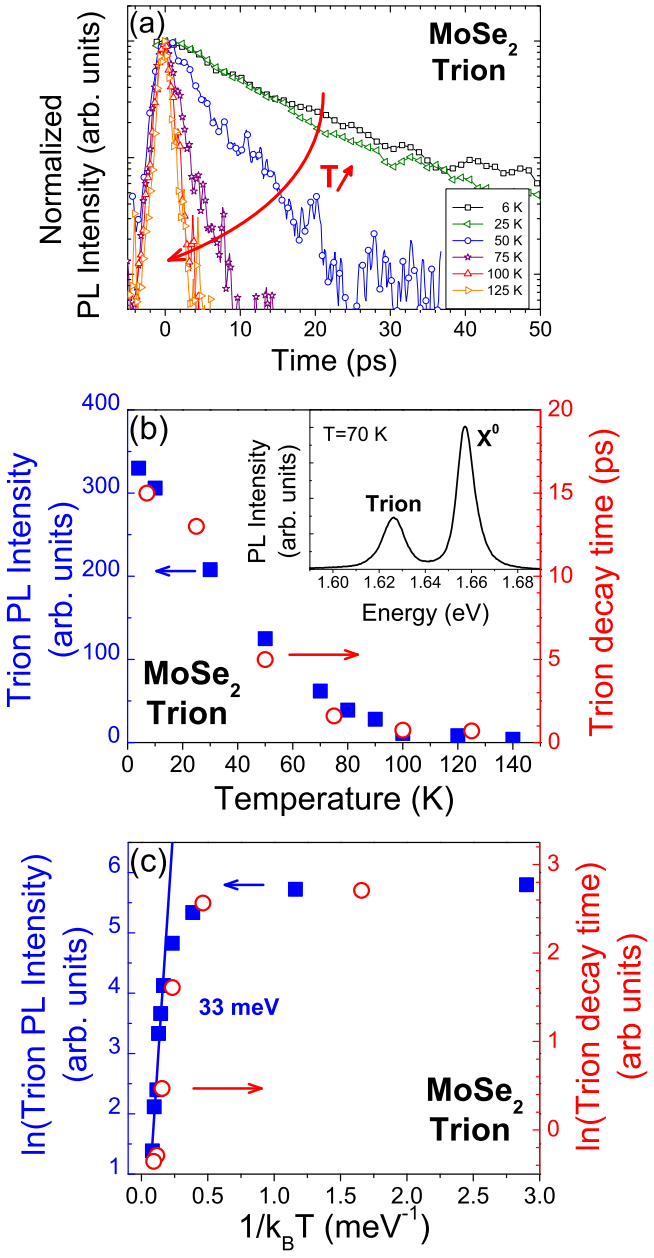

FIG. 6. (a) Trion photoluminescence dynamics for a $MoSe_2$ monolayer (ML C, $V = 0$ V) in the temperature range $T = 7 - 125$ K; above 125 K, the trion PL intensity vanishes. (b) Temperature dependence of the cw integrated PL intensity of the trion line (blue squares) and the trion PL decay time (red circles) obtained from a monoexponential fit of the trion kinetics measured in (a); inset: cw-photoluminescence spectrum of the $MoSe_2$ monolayer at $T = 70$ K. (c) Same data as in (b) in log scale in order to extract the activation energy ($E_A \sim 33$ meV).

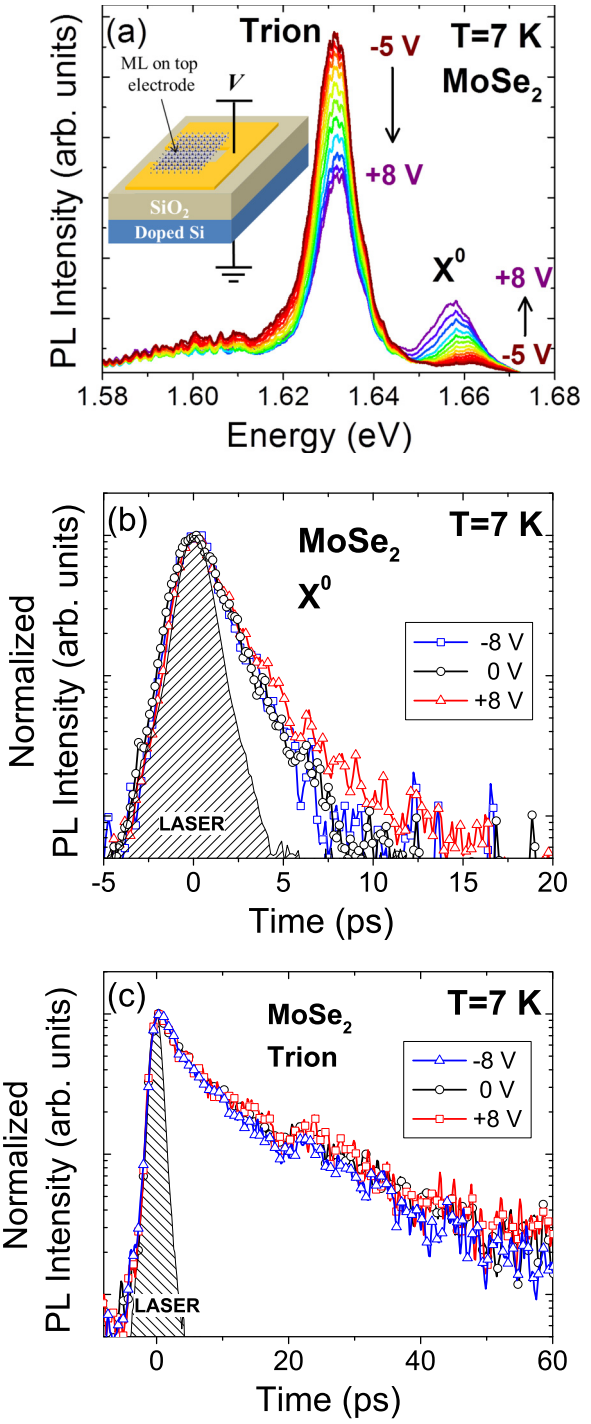

FIG. 7. (a) cw photoluminescence of the $MoSe_2$ monolayer (ML C) as a function of the gate voltage. Inset: sketch of the charge tunable device. The $MoSe_2$ ML is transferred with a PDMS stamp between two Cr/Au electrodes. Both electrodes are set to the same potential V while the doped Si substrate is grounded. (b) Exciton and trion (c) photoluminescence dynamics for three gate voltages at $T = 7$ K. The small hump at 20 ps comes from a small laser reflection in our setup.

InGaAs quantum wells, where the large increase of the trion formation time with temperature has been observed [73].

The interpretation of the exciton and trion dynamics is further supported by complementary experiments performed on ML C where the density of the resident electrons can be electrically tuned. As displayed in Fig. 7(a), the integrated luminescence intensity of the trion PL line decreases (with a simultaneous increase of the exciton line) when the applied voltage varies from -5 to 8 V as a result of a decrease of the resident electrons in the monolayer. Figures 7(b) and 7(c) show that the exciton and trion PL decay time at 7 K do not change significantly when the resident electrons density varies in this applied voltage range. This is again a strong indication

that the exciton and trion population decays independently and their radiative recombination times are so short that a dynamical equilibrium between the two species cannot be established. Let us emphasize that this conclusion applies for the quasiresonant excitation and the low temperature used here. Further investigations are required to check if this remains valid whatever the excitation energy is, for instance when the laser excitation energy lies above the free-carrier gap [30]. Temperature dependence would also be relevant. Unfortunately the voltage dependent measurements could not be performed for larger temperatures due to a strong increase of leakage currents in the device.

VII. DISCUSSION AND PROSPECTS

We have presented in the previous sections a scenario describing the time evolution of excitons from the initial nonthermal distribution following the quasi-resonant photogeneration to the thermal regime with two driving mechanisms: radiative recombination and exciton-phonon scattering.

The results and interpretations presented above are based on several assumptions which have to be discussed.

A. Exciton formation process

Though it is now recognized that excitons physics plays a crucial role on the optoelectronic properties of TMDC monolayers, the exciton formation dynamics has not been much studied. In inorganic semiconductors, two exciton formation processes are usually considered: (i) straight hot exciton photogeneration, with the simultaneous emission of LO phonons, in which the constitutive electron-hole pair is geminate; or (ii) bimolecular exciton formation which consists of the random binding of electrons and holes under the Coulomb interaction. Very few experimental results give a direct insight into the exciton formation processes. The geminate formation has been evidenced in polar semiconductors [74] whereas the second process was demonstrated in silicon, and led to the measurement of the bimolecular formation coefficient [75]. In GaAs quantum wells, several investigations also demonstrated the key role played by the bimolecular formation process [76–78].

In the present paper where we used quasiresonant excitation conditions, the excitation energy lies far below the free-carrier gap. Thus the exciton formation process is geminate as assumed in the previous sections.

Interestingly the measured exciton PL dynamics is very similar when the excitation energy is set below or above the free-carrier gap; see for instance Refs. [30,32–34] in MoS_2 or WSe_2 monolayers. For nonresonant excitation above the gap, the PL rise time is still very fast and no signature of bimolecular formation and energy relaxation of hot excitons can be evidenced, in contrast to III-V or II-VI quantum wells. As a consequence, we can speculate that the strong-exciton phonon coupling in TMDC monolayers yields a geminate exciton formation process whatever the excitation energy is.

B. Free and localized excitons dynamics

The TRPL experiments discussed in the previous sections have been interpreted on the basis of free exciton recombination though the PL emission lines are clearly inhomogeneously broadened [FWHM $\sim$10 meV at $T = 4$ K; see Fig. 1(a)]. In contrast the measurement of intrinsic radiative lifetime of free excitons in III–V and II–VI quantum wells could only be observed in high quality samples with narrow linewidths dominated by homogenous broadening [59,60]. For excitons in lower quality samples with Stokes shift of a few meV (energy difference between emission and absorption exciton peaks), localization and scattering processes usually yield much longer decay times of luminescence [65]. In the TMDC ML investigated in this paper, we did not measure any significant Stokes shift. This is a solid hint to believe that such a strong exciton localization may not occur in TMDC ML. Nevertheless, we cannot exclude the presence of other localization effects in TMDC ML as we observe a significant discrepancy between the measured intrinsic radiative lifetime (1.8 ps see Sec. IV) and the theoretical time expected for free excitons (0.3 ps) given by Eq. (1). To identify such a localization mechanism, we need to compare the exciton Bohr radius (which is much smaller in TMDC ML ($\sim$0.5 nm) than in GaAs quantum wells ($\sim$10 nm)), with the correlation length of in-plane potential fluctuations. Unfortunately, these fluctuations are not known in 2D materials based on TMDC; it could possibly be investigated in the future with near-field techniques.

C. Role of dark excitons

The excitons dynamics in TMDC monolayer can depend critically on the interplay between bright and dark excitons. Basically three different kinds of excitons can be termed "dark":

(i) The spin-allowed Γ excitons with wave vectors $k > k_0$, which lie above the radiative window (Fig. 4). These dark excitons were fully considered in the previous sections.

(ii) The spin-forbidden dark excitons in the Γ zone center, which lie 10–30 meV above the spin-allowed optical transitions for $MoSe_2$ ML [see dashed line in Fig. 4(a)]. At low temperatures $T \lesssim 100$ K, we did not observe any interplay between these dark excitons and the bright ones which decay radiatively. For larger temperatures, a dynamical equilibrium between these bright and dark excitons could arise but the simultaneous increase of nonradiative recombination channels prevent us from observing any evidence of it. We emphasize that Eq. (2) assumes such an equilibrium [if there is no equilibrium, $\tau_{\mathrm{rad}}^{\mathrm{eff}}$ must be divided by a factor 2 in Eq. (2) [45]].

(iii) Indirect excitons: in addition to the dark excitons (i) and (ii) which have been evidenced in many semiconductor bulk and nanostructures, the D_{3h} symmetry of TMDC monolayer requires us to consider a third type of dark excitons. As the carriers can populate the two nonequivalent K_+ and K_- valley (characterized by opposite spin-orbit splitting), an exciton can be formed with a conduction-band and a valence-band state lying in opposite valleys [70]. The lowest indirect excitons cannot recombine radiatively since they are spin forbidden. In fact, at $T = 7$ K, we did not observe any fingerprint of these dark indirect excitons. At higher temperature, higher energy spin-allowed dark excitons recombination may be possible by simultaneous phonon emission or absorption. We can speculate that they could constitute an

additional reservoir of dark excitons which should again lead to the observation of longer photoluminescence component associated to the relaxation from the K to Γ valley. Crucial information such as the binding and exchange energy of such excitons are desirable in order to progress in our understanding of the role of these indirect excitons on the luminescence dynamics.

VIII. CONCLUSION

We have investigated the exciton radiative recombination dynamics in TMDC monolayers by time-resolved photoluminescence experiments with optimized time resolution. The time evolution of the luminescence intensity in the very first picoseconds at low temperature provides precious information on the nonthermal dynamics of excitons. Ultrafast intrinsic radiative recombination times ($\sim$2 ps) are measured for both $MoSe_2$ and WSe_2 monolayers. The temperature dependence of the luminescence decay times allows us to reveal the complex exciton dynamics controlled by the effective radiative recombination time, very efficient exciton-phonon scattering, exciton-exciton interactions, as well as the interplay between the bright excitons and the various kinds of nonoptically active excitons. In the future the measurement of the homogeneous linewidth with four-wave mixing spectroscopy in monolayers where the exciton and trion lines are well resolved should help us to fully understand these complex radiative recombination processes in transition metal dichalcogenides.

ACKNOWLEDGMENTS

The authors thank J.Roux from the Hamamatsu company for the loan of a synchroscan Streak Camera C10910 with a 0.9-ps time resolution and Benoit Chalopin and Sébastien Weber from the LCAR for the loan of the autocorrelator. We are grateful to M. Glazov for useful discussions. We thank the ANR MoS2ValleyControl and Programme Investissements d'Avenir ANR-11-IDEX-0002-02, reference ANR-10-LABX-0037-NEXT, and ERC Grant No. 306719 for financial support. X.M. also acknowledges the Institut Universitaire de France.

[1] K. F. Mak, C. Lee, J. Hone, J. Shan, and T. F. Heinz, Phys. Rev. Lett. **105**, 136805 (2010).
[2] A. Splendiani, L. Sun, Y. Zhang, T. Li, J. Kim, C.-Y. Chim, G. Galli, and F. Wang, Nano Lett. **10**, 1271 (2010).
[3] R. S. Sundaram, M. Engel, A. Lombardo, R. Krupke, A. C. Ferrari, Ph. Avouris, and M. Steiner, Nano Lett. **13**, 1416 (2013).
[4] Y. Ye, Z. Ye, M. Gharghi, H. Zhu, M. Zhao, Y. Wang, X. Yin, and X. Zhang, Appl. Phys. Lett. **104**, 193508 (2014).
[5] O. Lopez-Sanchez, E. Alarcon Llado, V. Koman, A. Fontcuberta i Morral, A. Radenovic, and A. Kis, ACS Nano **8**, 3042 (2014).
[6] S. Wu, S. Buckley, J. R. Schaibley, L. Feng, J. Yan, D. G. Mandrus, F. Hatami, W. Yao, J. Vučković, A. Majumdar, and X. Xu, Nature (London) **520**, 69 (2015).
[7] Y. Ye, Z. J. Wong, X. Lu, X. Ni, H. Zhu, X. Chen, Y. Wang, and X. Zhang, Nat. Photon. **9**, 733 (2015).
[8] D. Xiao, G.-B. Liu, W. Feng, X. Xu, and W. Yao, Phys. Rev. Lett. **108**, 196802 (2012).
[9] T. Cao, G. Wang, W. Han, H. Ye, C. Zhu, J. Shi, Q. Niu, P. Tan, E. Wang, B. Liu *et al.*, Nat. Commun. **3**, 887 (2012).
[10] G. Sallen, L. Bouet, X. Marie, G. Wang, C. R. Zhu, W. P. Han, Y. Lu, P. H. Tan, T. Amand, B. L. Liu *et al.*, Phys. Rev. B **86**, 081301 (2012).
[11] K. F. Mak, K. He, J. Shan, and T. F. Heinz, Nat. Nanotechnol. **7**, 494 (2012).
[12] Kioseoglou, A. T. Hanbicki, M. Currie, A. L. Friedman, D. Gunlycke, and B. T. Jonker, Appl. Phys. Lett. **101**, 221907 (2012).
[13] T. Cheiwchanchamnangij and W. R. L. Lambrecht, Phys. Rev. B **85**, 205302 (2012).
[14] H.-P. Komsa and A. V. Krasheninnikov, Phys. Rev. B **86**, 241201 (2012).
[15] K. He, N. Kumar, L. Zhao, Z. Wang, K. F. Mak, H. Zhao, and J. Shan, Phys. Rev. Lett. **113**, 026803 (2014).
[16] M. M. Ugeda, A. J. Bradley, S.-F. Shi, F. H. da Jornada, Y. Zhang, D. Y. Qiu, S.-K. Mo, Z. Hussain, Z.-X. Shen, F. Wang *et al.*, Nat. Mater. **13**, 1091 (2014).
[17] A. Chernikov, T. C. Berkelbach, H. M. Hill, A. Rigosi, Y. Li, O. B. Aslan, D. R. Reichman, M. S. Hybertsen, and T. F. Heinz, Phys. Rev. Lett. **113**, 076802 (2014).
[18] Z. Ye, T. Cao, K. O'Brien, H. Zhu, X. Yin, Y. Wang, S. G. Louie, and X. Zhang, Nature (London) **513**, 214 (2014).
[19] G. Wang, X. Marie, I. Gerber, T. Amand, D. Lagarde, L. Bouet, M. Vidal, A. Balocchi, and B. Urbaszek, Phys. Rev. Lett. **114**, 097403 (2015).
[20] X. Liu, T. Galfsky, Z. Sun, F. Xia, E. Lin, Y.-H. Lee, S. Kéna-Cohen, and V. M. Menon, Nat. Photon. **9**, 30 (2015).
[21] S. Dufferwiel, S. Schwarz, F. Withers, A. A. P. Trichet, F. Li, M. Sich, O. Del Pozo-Zamudio, C. Clark, A. Nalitov, D. D. Solnyshkov, G. Malpuech, K. S. Novoselov, J. M. Smith, M. Skolnick, D. N. Krizhanovskii, and A. I. Tartakovskii, Nat. Commun. **6**, 8579 (2015).
[22] A. Singh, G. Moody, S. Wu, Y. Wu, N. J. Ghimire, J. Yan, D. G. Mandrus, X. Xu, and X. Li, Phys. Rev. Lett. **112**, 216804 (2014).
[23] C. Mai, A. Barrette, Y. Yu, Y. G. Semenov, K. W. Kim, L. Cao, and K. Gundogdu, Nano Lett. **14**, 202 (2014).
[24] N. Kumar, Q. Cui, F. Ceballos, D. He, Y. Wang, and H. Zhao, Nanoscale **6**, 4915 (2014).
[25] C. R. Zhu, K. Zhang, M. Glazov, B. Urbaszek, T. Amand, Z. W. Ji, B. L. Liu, and X. Marie, Phys. Rev. B **90**, 161302(R) (2014).
[26] C. Poellmann, P. Steinleitner, U. Leierseder, P. Nagler, G. Plechinger, M. Porer, R. Bratschitsch, C. Schüller, T. Korn, and R. Huber, Nat. Mater. **14**, 889 (2015).
[27] Q. Wang, S. Ge, X. Li, J. Qiu, Y. Ji, J. Feng, and D. Sun, ACS Nano **7**, 11087 (2013).
[28] H. Shi, R. Yan, S. Bertolazzi, J. Brivio, B. Gao, A. Kis, D. Jena, H. G. Xing, and L. Huang, ACS Nano **7**, 1072 (2013).
[29] S. Mouri, Y. Miyauchi, M. Toh, W. Zhao, G. Eda, and K. Matsuda, Phys. Rev. B **90**, 155449 (2014).
[30] X.-X. Zhang, Y. You, S. Y. F. Zhao, and T. F. Heinz, Phys. Rev. Lett. **115**, 257403 (2015).
[31] T. Yan, X. Qiao, X. Liu, P. Tan, and X. Zhang, Applied Phys. Lett. **105**, 101901 (2014).

[32] T. Korn, S. Heydrich, M. Hirmer, J. Schmutzler, and C. Schüller, Appl. Phys. Lett. **99**, 102109 (2011).

[33] D. Lagarde, L. Bouet, X. Marie, C. R. Zhu, B. L. Liu, T. Amand, P. H. Tan, and B. Urbaszek, Phys. Rev. Lett. **112**, 047401 (2014).

[34] G. Wang, L. Bouet, D. Lagarde, M. Vidal, A. Balocchi, T. Amand, X. Marie, and B. Urbaszek, Phys. Rev. B **90**, 075413 (2014).

[35] G. Wang, E. Palleau, T. Amand, S. Tongay, X. Marie, and B. Urbaszek, Appl. Phys. Lett. **106**, 112101 (2015).

[36] H. Wang, C. Zhang, W. Chan, C. Manolatou, S. Tiwari, and F. Rana, Phys. Rev. B **93**, 045407 (2016).

[37] M. Palummo, M. Bernardi, and J. C. Grossman, Nano Lett. **15**, 2794 (2015).

[38] G. Wang, C. Robert, A. Suslu, B. Chen, S. Yang, S. Alamdari, I. C. Gerber, T. Amand, X. Marie, S. Tongay, and B. Urbaszek, Nat. Commun. **6**, 10110 (2015).

[39] A. Arora, K. Nogajewski, M. Molas, M. Koperski, and M. Potemski, Nanoscale **7**, 20769 (2015).

[40] F. Withers, O. Del Pozo-Zamudio, S. Schwarz, S. Dufferwiel, P. M. Walker, T. Godde, A. P. Rooney, A. Gholinia, C. R. Woods, P. Blake *et al.*, Nano Lett. **15**, 8223 (2015).

[41] N. Kumar, Q. Cui, F. Ceballos, D. He, Y. Wang, and H. Zhao, Phys. Rev. B **89**, 125427 (2014).

[42] J. S. Ross, S. Wu, H. Yu, N. J. Ghimire, A. M. Jones, G. Aivazian, J. Yan, D. G. Mandrus, D. Xiao, W. Yao, and X. Xu, Nat. Commun. **4**, 1474 (2013).

[43] G. Wang, I. C. Gerber, L. Bouet, D. Lagarde, A. Balocchi, M. Vidal, T. Amand, X. Marie, and B. Urbaszek, 2D Mater. **2**, 045005 (2015).

[44] Y. Li, A. Chernikov, X. Zhang, A. Rigosi, H. M. Hill, A. M. van der Zande, D. A. Chenet, E.-M. Shih, J. Hone, and T. F. Heinz, Phys. Rev. B **90**, 205422 (2014).

[45] L. C. Andreani, Solid State Commun. **77**, 641 (1991).

[46] M. M. Glazov, E. L. Ivchenko, G. Wang, T. Amand, X. Marie, B. Urbaszek, and B. L. Liu, Phys. Status Solidi B **252**, 2349 (2015).

[47] G. Moody, C. K. Dass, K. Hao, C. H. Chen, L. J. Li, A. Singh, K. Tran, G. Clark, X. Xu, G. Berghauser, E. Malic, A. Knorr, and X. Li, Nat. Commun. **6**, 8315 (2015).

[48] K. Kósmider, J. W. González, and J. Fernández-Rossier, Phys. Rev. B **88**, 245436 (2013).

[49] A. Molina-Sánchez, D. Sangalli, K. Hummer, A. Marini, and L. Wirtz, Phys. Rev. B **88**, 045412 (2013).

[50] J. P. Echeverry, B. Urbaszek, T. Amand, X. Marie, and I. C. Gerber, Phys. Rev. B **93**, 121107 (2016).

[51] M. D. McGehee and A. J. Heeger, Adv. Mater. **12**, 1655 (2000).

[52] D. Sun, Y. Rao, G. A. Reider, G. Chen, Y. You, L. Brézin, A. R. Harutyunyan, and T. F. Heinz, Nano Lett. **14**, 5625 (2014).

[53] M. Amani, D.-H. Lien, D. Kiriya, J. Xiao, A. Azcatl, J. Noh, S. R. Madhvapathy, R. Addou, S. KC, M. Dubey, K. Cho, R. M. Wallace, S.-C. Lee, Jr.-H. He, J. W. Ager III, X. Zhang, E. Yablonovitch, and A. Javey, Science **350**, 1065 (2015).

[54] H.-V. Han, A.-Y. Lu, L.-S. Lu, J.-K. Huang, H. Li, C.-L. Hsu, Y.-C. Lin, M.-H. Chiu, K. Suenaga, C.-W. Chu, H.-C. Kuo, W.-H. Chang, L.-J. Li, and Y. Shi, ACS Nano **10**, 1454 (2015).

[55] P. Tonndorf, R. Schmidt, P. Böttger, X. Zhang, J. Börner, A. Liebig, M. Albrecht, C. Kloc, O. Gordan, D. R. T. Zahn, S. Michaelis de Vasconcellos, and R. Bratschitsch, Opt. Express **21**, 4908 (2013).

[56] S. Tongay, J. Zhou, C. Ataca, K. Lo, T. S. Matthews, J. Li, J. C. Grossman, and J. Wu, Nano Lett. **12**, 5576 (2012).

[57] G. Wang, M. M. Glazov, C. Robert, T. Amand, X. Marie, and B. Urbaszek, Phys. Rev. Lett. **115**, 117401 (2015).

[58] A. M. Jones, H. Yu, J. R. Schaibley, J. Yan, D. G. Mandrus, T. Taniguchi, K. Watanabe, H. Dery, W. Yao, and X. Xu, Nat. Phys. **12**, 323 (2016).

[59] B. Deveaud, F. Clérot, N. Roy, K. Satzke, B. Sermage, and D. S. Katzer, Phys. Rev. Lett. **67**, 2355 (1991).

[60] A. Vinattieri, J. Shah, T. C. Damen, D. S. Kim, L. N. Pfeiffer, M. Z. Maialle, and L. J. Sham, Phys. Rev. B **50**, 10868 (1994).

[61] A. V. Trifonov, S. N. Korotan, A. S. Kurdyubov, I. Ya. Gerlovin, I. V. Ignatiev, Yu. P. Efimov, S. A. Eliseev, V. V. Petrov, Yu. K. Dolgikh, V. V. Ovsyankin, and A. V. Kavokin, Phys. Rev. B **91**, 115307 (2015).

[62] E. Vanelle, M. Paillard, X. Marie, T. Amand, P. Gilliot, D. Brinkmann, R. Levy, J. Cibert, and S. Tatarenko, Phys. Rev. B **62**, 2696 (2000).

[63] D. Y. Qiu, F. H. da Jornada, and S. G. Louie, Phys. Rev. Lett. **111**, 216805 (2013).

[64] J. Hegarty, L. Goldner, and M. D. Sturge, Phys. Rev. B **30**, 7346 (1984).

[65] X. Marie, F. Lephay, T. Amand, J. Barrau, and F. Voillot, Superlattices Microstruct. **10**, 415 (1991).

[66] A. Honold, L. Schultheis, J. Kuhl, and C. W. Tu, Phys. Rev. B **40**, 6442 (1989).

[67] A. Vinattieri, F. Bogani, L. Cavigli, D. Manzi, M. Gurioli, E. Feltin, J.-F. Carlin, D. Martin, R. Butté, and N. Grandjean, Phys. Rev. B **87**, 075202 (2013).

[68] Y. Yu, Y. Yu, C. Xu, A. Barrette, K. Gundogdu, and L. Cao, arXiv:1512.00945.

[69] A. Singh, G. Moody, K. Tran, M. E. Scott, V. Overbeck, G. Berghäuser, J. Schaibley, E. J. Seifert, D. Pleskot, N. M. Gabor, J.Yan, D. G. Mandrus, M. Richter, E. Malic, X. Xu, and X. Li, Phys. Rev. B **93**, 041401 (2016).

[70] H. Dery and Y. Song, Phys. Rev. B **92**, 125431 (2015).

[71] S.-Y. Chen, C. Zheng, M. S. Fuhrer, and J. Yan, Nano Lett. **15**, 2526 (2015).

[72] S. Horzum, H. Sahin, S. Cahangirov, P. Cudazzo, A. Rubio, T. Serin, and F. M. Peeters, Phys. Rev. B **87**, 125415 (2013).

[73] M. T. Portella-Oberli, J. Berney, L. Kappei, F. Morier-Genoud, J. Szczytko, and B. Deveaud-Pledran, Phys. Rev. Lett. **102**, 096402 (2009).

[74] A.Bonnot, R. Planel, and C. Benoît a la Guillaume, Phys. Rev. B **9**, 690 (1974).

[75] J. Barrau, M. Heckmann, and M. Brousseau, J. Phys. Chem. Solids **34**, 381 (1973).

[76] T. Amand, B. Dareys, B. Baylac, X. Marie, J. Barrau, M. Brousseau, D. J. Dunstan, and R. Planel, Phys. Rev. B **50**, 11624 (1994).

[77] J. Szczytko, L. Kappei, J. Berney, F. Morier-Genoud, M. T. Portella-Oberli, and B. Deveaud, Phys. Rev. Lett. **93**, 137401 (2004).

[78] D. Robart, X. Marie, B. Baylac, T. Amand, M. Brousseau, G. Bacquet, and G. Debart, Solid State Commun. **95**, 287 (1995).